Spin-reorientation in $ErFeO_3$: Zero-field transitions, three-dimensional phase diagram, and anisotropy of erbium magnetism

Ya. B. Bazaliy,[1] L. T. Tsymbal,[2,3,*] G. N. Kakazei,[3] A. I. Izotov,[2] and P. E. Wigen[3]
[1]*Argonne National Laboratory, Materials Science Division, 9700 S. Cass Avenue, Argonne, Illinois 60439, USA*
[2]*O. Galkin Donetsk Physics & Technology Institute, National Academy of Sciences Ukraine, R. Luxemburg Street 72, Donetsk, 83114 Ukraine*
[3]*Department of Physics, Ohio State University, 174 W. 18th Avenue Columbus, Ohio 43210, USA*
(Received 25 June 2003; revised manuscript received 23 September 2003; published 26 March 2004)

Spontaneous spin-reorientation transitions in $ErFeO_3$ are studied using ultrasound, magnetic susceptibility, and magnetic moment measurements. The properties of the first-order transition happening in magnetic field sweeps through zero are studied and a three-dimensional (H,T) magnetic phase diagram of the material is constructed. Direct measurements of the magnetic moment allow for a precise determination of the temperature dependence of the magnetization direction in the reorientation region. The mean-field theory of orientation transitions is modified to account for the magnetism of the erbium subsystem, and an excellent agreement with experiment is achieved.

DOI: 10.1103/PhysRevB.69.104429 PACS number(s): 75.30.Kz, 75.50.Dd, 75.60.−d

I. INTRODUCTION

Orthoferrite $ErFeO_3$ belongs to the family of rhombic rare-earth orthoferrites, which were first identified in the early 1940s and became a subject of extensive studies by many research groups (see, e.g., Refs. 1–3). They have the chemical formula $RFeO_3$, where R is a rare-earth ion. A characteristic feature of the $RFeO_3$ is the presence of two magnetic subsystems, the rare-earth ions and the iron ions.

The iron subsystem usually orders magnetically at the Neel temperature $T_N \sim 620-740$ K into a slightly canted antiferromagnetic structure with the Neel vector **G** and the ferromagnetic vector **F**. The ferromagnetic moment is usually very small, but plays an important role in the phenomena discussed in this paper.

As a rule the rare-earth subsystem orders magnetically below $T_{NR} \approx 5-10$ K. Above this temperature the R ions are paramagnetic, but experience the molecular field of the iron subsystem which partially magnetizes them.[1,4–8] Magnetic moment of erbium subsystem will be denoted by **m**. Consequently the total magnetic moment is $\mathbf{M}=\mathbf{F}+\mathbf{m}$.

The iron and rare-earth subsystems have quite different properties, which can change with temperature, field, or elastic stress. They also interact with one another. It was found that this interaction leads to a whole series of orientation phase transitions (OPT), in which the spin system rotates with respect to the crystal axis. These transitions are studied in both bulk materials and films (see Refs. 1–3 and references therein, and more recent work[9–12]).

When iron orders at T_N, its magnetic structure corresponds to the irreducible representation Γ_4 (G_x,F_z) with **F** pointing along the **c** axis of the crystal (the z coordinate axis is chosen along **c**). All orthoferrites order with $\mathbf{F}\|\mathbf{c}$ immediately below the Néel temperature. This phase is known as a major phase. It is also called the symmetric phase because the magnetic moment points along one of the symmetry axis of the crystal. For nonmagnetic rare earths R = La, Y, Lu this phase persists to the lowest temperatures. For other rare-earth ions magnetic reorientation transitions occur upon cooling. The most common type of spin reorientation is a sequence of transitions $\Gamma_4(G_x,F_z) \rightarrow \Gamma_{24}(G_{x,z},F_{x,z}) \rightarrow \Gamma_2(G_z,F_x)$ which brings the system to another symmetric configuration Γ_2 with $\mathbf{F}\|\mathbf{a}$ (the x coordinate axis is chosen along **a**) through the intermediate Γ_{24} tilted phase. The $\Gamma_4 \rightarrow \Gamma_{24}$ and $\Gamma_{24} \rightarrow \Gamma_2$ transitions are two second-order orientation phase transitions. Their temperatures are denoted as T_1 and T_2 $(T_2<T_1<T_N)$. The overall picture of the transition is as follows: upon cooling down from T_N, the first spontaneous OPT happens at temperature T_1, where vector **F** starts to rotate from **c** axis towards the **a** axis staying in the (**a**,**c**) plane. Rotations happens in the temperature interval $T \in [T_2,T_1]$, i.e., in the tilted Γ_{24} phase. At T_2 vector **F** reaches the **a** direction and rotation stops. This is the point of another spontaneous OPT. It happens in many orthoferrites, e.g., for R = Tm, Er, Yb, Sm, Nd and in a somewhat different form for R = Ho. In the tilted phase the whole antiferromagnetic structure continuously rotates, for example, vector **F** rotates in the (**a**,**c**) crystal plane from the **c** axis to **a** axis. In the Landau theory approach these transitions are often described by the temperature dependence of the anisotropy constants of iron subsystem.[13–19] The reorientation temperature interval $[T_2,T_1]$ can differ greatly for different rare earths. For example, in $YbFeO_3$ $T_2 \approx 6.8$ K, $T_1 \approx 8$ K, while in $SmFeO_3$ $T_2 \approx 450$ K, $T_1 \approx 478$ K. In this paper the reorientation phase transitions in $ErFeO_3$ for which $T_2 \approx 88$ K, $T_1 \approx 97$ K is studied. Approximate equalities are used because transition temperatures turn out to be sensitive to crystal growth and other conditions and can differ from sample to sample.[15,20]

Since in $ErFeO_3$ OPT's happen at a temperature much lower than T_N, the iron sublattice magnetizations are almost fully saturated. It is assumed that during the OPT they simply rotate, retaining the same absolute value. Moreover, it is proved that when the transition occurs in the absence of an external magnetic field (spontaneous OPT), the angle between the sublattice magnetizations remains constant as they

rotate together. In this case it is enough to follow the rotation of vector **F** to describe the transition. Such description may no longer be sufficient in very high magnetic fields, which pull sublattice magnetization towards the field direction eventually inducing the spin-flip transition. However these regimes will not be discussed here.

When external magnetic field **H** is applied, it couples to vector **F** and may change it. For the moderate fields used in this study the magnitude of **F** is not influenced by *H*. Thus it is still not necessary to take into account the full antiferromagnetic structure of $ErFeO_3$ and the evolution of **F** can be followed. The magnetic field produces an additional rotation of **F** on top of the spontaneous rotation discussed above. It was shown that for $\mathbf{H}\|\mathbf{c}$ and $\mathbf{H}\|\mathbf{a}$ one observes field-induced second-order OPTs at finite fields $H_{a,c}(T)$.[3,13,14,21] If the magnetic field is pointing in an arbitrary direction in the (**a**,**c**) plane, not exactly along **a**- or **c**-axis, no induced transition happens. Here for the first time the (H_a,T) and (H_c,T) phase diagrams were combined in a three-dimensional (3D) (H_a,H_c,T) phase diagram of the orthoferrite. The obtained 3D diagram shows that crossing the $H=0$ point in a field sweep results in a first-order OPT for almost all directions of **H**. These first order OPT's will be the primary subject of this investigation.

In this work the OPT's in $ErFeO_3$ were studied by measuring the magnetic susceptibility, ultrasound velocity, and magnetic moment. The combination of these methods allow a precise measurement of the $T_{1,2}$ temperatures.

Then, the transition that happens when a magnetic field is swept through $H=0$ was investigated. Like for any first-order magnetic transition, its observation was complicated by the emergence of magnetic domains. With a proper interpretation, the results confirmed our generalization of the magnetic phase diagram. The magnetization loops observed in the tilted and symmetric phases are described in the text, and the influence of the domain structure on their formation is discussed.

Finally, a systematic study of the spin rotation angle $\theta(T)$ between **M** and **c** axis in the (T_1,T_2) interval at zero magnetic field was performed. This is done by a direct magnetic moment measurement using a superconducting quantum interference device (SQUID) magnetometer. Data on $\theta(T)$ in $ErFeO_3$ are scarce in the literature: most investigators concentrated on other rare-earth orthoferrites. The only earlier measurements we are aware of are the nuclear-magnetic-resonance (NMR) study[22] and Mossbauer measurement[23] from which the $\theta(T)$ dependence was extracted in the framework of a certain models. Our study offers a direct and more accurate experimental determination of the tilting angle and sufficiently differs from Refs. 22 and 23. The temperature dependence $\theta(T)$ obtained in our experiment does not follow previous theoretical predictions,[3,6,13,14,17–19,21] but was reproduced well by a modified mean-field theory developed in this paper. Temperature dependencies of the rotation angle were also measured before for $YbFeO_3$ (Ref. 21) and $SmFeO_3$.[24] The results were at best in partial agreement with the theories used to interpret them.

II. EXPERIMENT

All measurements were performed on samples prepared from single crystals of $ErFeO_3$ that were grown by the floating-zone method using radiation-induced melting in a setup without a crucible.

Ultrasound measurements and magnetic susceptibility measurements were done on a cylinder sample with rounded edges. The sample was 4 mm in diameter and 1.9 mm high. The **c** axis was aligned along the cylinder axis with the accuracy of 0.5 deg. Magnetic moment measurements in a SQUID magnetometer were done on a rectangular sample with rounded edges and corners. Its dimensions are $3.9\times3.1\times3.9\ \mathrm{mm}^3$. Its weight is 0.405 g. The sides of the rectangle coincided with the **a** and **c** axis with the accuracy of 0.5 deg.

Acoustic studies were conducted using a pulsed ultrasonic spectrometer. A purely transverse sound mode with 25 MHz frequency was excited by a specially designed transducer made of $LiNbO_3$. A phase-sensitive technique was used to measure relative sound velocity changes. The accuracy of such measurements is 10^{-6}. Temperature was measured with a copper thermometer located near the sample.

The magnetic susceptibility diverges near the OPT points as $\chi\sim1/\sqrt{T-T_{1,2}}$. It was measured with an autodyne generator operating at 6.2 MHz base frequency in a setup analogous to the NMR spectrometer. The resonance frequency ν of the generator is very sensitive to the susceptibility of the sample, $\nu\sim1/\sqrt{1+4\pi\chi}$. It was measured with a 10^{-8} relative error. The sample was placed directly on a flat spiral coil coupled to the autodyne generator. The rf field of the coil permits the record of a χ_a and χ_c combination and divergence of either susceptibility could be observed in the same experimental run. The temperature was measured by a thermal emf of a copper-constantan pair.

The dc value of magnetic moment was measured using a SQUID magnetometer quantum design MPMS-5S in the temperature range from 75 to 105 K and in magnetic fields up to 300 Oe. Measurements of the magnetic moment as a function of temperature were performed both in zero magnetic field and at 50 Oe.

III. RESULTS

Figure 1 shows the temperature dependence of the relative change of the sound velocity *S* for the transverse mode with wave vector $\mathbf{k}||\mathbf{c}$ and polarization vector $\varepsilon||\mathbf{a}$. This mode was chosen because symmetry considerations[25,26] show that it must be softened during the $\Gamma_2\rightarrow\Gamma_{24}\rightarrow\Gamma_4$ transitions.

Near the transitions a decrease of *S* is observed. These anomalies show no hysteresis upon decreasing and increasing the temperature and are in accord with the theory.[27,26] The other transverse mode $(\varepsilon||\mathbf{b})$ with the same wave vector shows miniscule changes of *S*.

Figure 2 shows the behavior of magnetic susceptibility in the same temperature interval. No hysteresis is observed and the shape of the observed anomalies follows the theoretical predictions as well. To sum up, both orientation phase tran-

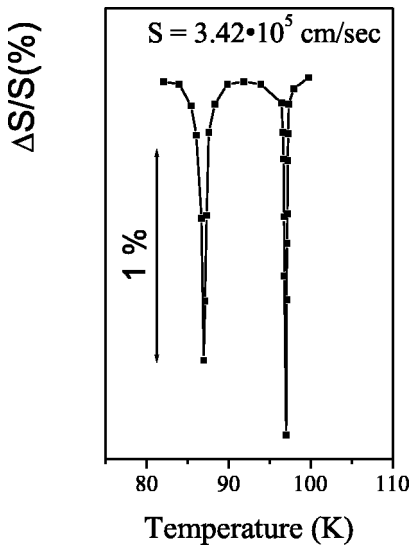

FIG. 1. Temperature dependence of the sound velocity of the transverse sound mode with the wave vector $\mathbf{k}\|\mathbf{c}$ and polarization vector $\varepsilon||\mathbf{a}$. The relative change of S displays anomalies at the OPT points.

sitions at $T_1=97$ K and $T_2=88$ K are clearly seen and their second-order nature is confirmed.

Next, the magnetic moment $\mathbf{M}$ of the $ErFeO_3$ sample is measured in the reorientation temperature interval. The SQUID magnetometer measurements were performed as follows. First, at each temperature point a saturating magnetic field $H=300$ Oe was applied in either **a** or **c** axis. Then, the field was reduced to zero and the projection of the remnant magnetic moment $\mathbf{M}^{\text{remnant}}$ on the same axis was measured. Two series of measurements, one for $\mathbf{M}_c^{\text{remnant}}$ and another for $\mathbf{M}_a^{\text{remnant}}$ were made.

The results are shown in Fig. 3. At first they seem to be in contradiction with the picture of a continuous rotation of $\mathbf{M}$

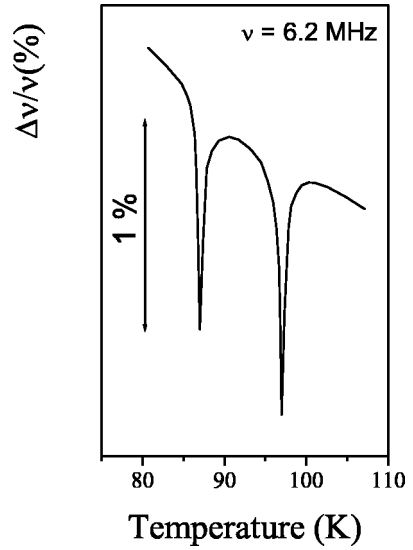

FIG. 2. Temperature dependence of the autodyne generator frequency shift. Anomalies of $\Delta\nu/\nu$ reflect the anomalies of magnetic susceptibility χ and correspond to the OPT points.

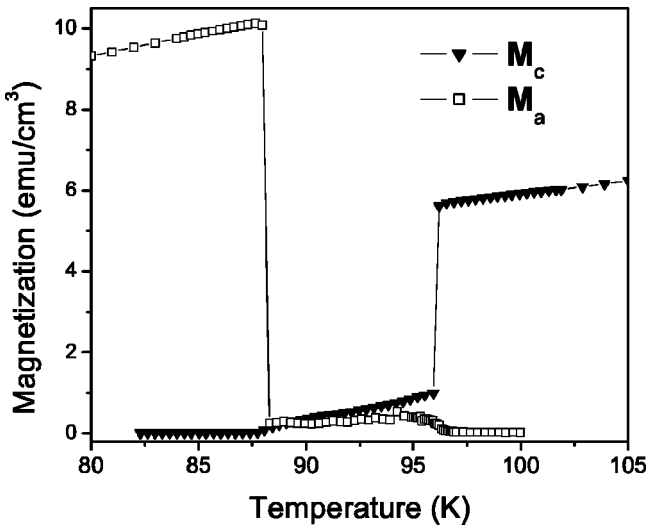

FIG. 3. Zero magnetic field value of the remnant magnetic moment $\mathbf{M}^{\text{remnant}}(T)$. At each temperature a saturating field of 300 Oe was applied along **a** or **c** axis and reduced to zero (see text). Component along **a** axis is shown with squares and along **c** axis with triangles.

in the tilted phase, since the absolute value of $\mathbf{M}$ seems to be very close to zero in the $[T_2,T_1]$ interval. This issue will be clarified later by further measurements. The main point here is that Fig. 3 shows a sharp distinction in the magnetic moment behavior for three intervals $T>T_1$, $T_2<T<T_1$, and $T<T_2$. As it will be explained below, the value of $\mathbf{M}^{\text{remnant}}$ in the reorientation region is not particularly useful. But from the high- and low-temperature data it should be noted that the magnetic moment in Γ_2 phase is larger than in Γ_4 phase. This is a manifestation of the behavior of the rare-earth magnetic moments. The degree of their partial magnetization by the molecular field of the ordered iron subsystem changes during the reorientation process. This question is discussed in detail in the following section.

To clarify the situation in the reorientation regions, hysteresis loops were measured throughout this temperature range. A series of $M(H)$ loops is shown in Fig. 4(a) for $\mathbf{H}\|\mathbf{a}$ and Fig. 4(b) for $\mathbf{H}\|\mathbf{c}$. From Fig. 4(b) for temperatures sufficiently above T_1 a rectangular hysteresis loop is observed. As the temperature approaches T_1, the shape of the loop changes from square to triangular. Finally the loop becomes an S-shaped curve without hysteresis for temperatures deep in the reorientation region. Below T_2 the $M(H)$ dependence is a straight line with the slope corresponding to the paramagnetic contribution of Er ions.

Similarly, Fig. 4(a), for $\mathbf{H}\|\mathbf{a}$ square loops are observed for $T<T_2$. Around T_2 they transform into triangular loops and then become S-shaped curves without hysteresis deep in the reorientation region. Finally, a straight line is observed for $T>T_1$.

The shape of the loops in the symmetric phases Γ_2 and Γ_4 can be explained by assuming that magnetic domains are not formed and the sample magnetization switches coherently. This explains the square loops and implies that the $\mathbf{M}^{\text{remnant}}$ measurement gives a reliable measure of the saturation mag-

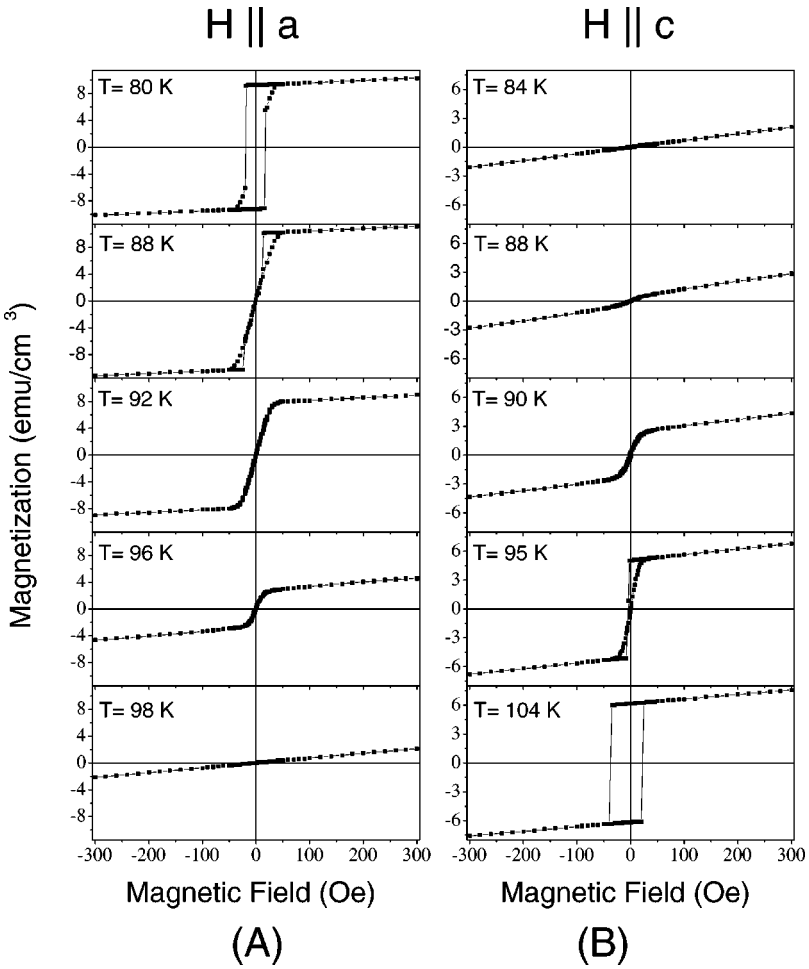

FIG. 4. Magnetization loops $M(H)$ for symmetric directions of the external field. (a) magnetic field along the **a** axis, (b) magnetic field along the **c** axis.

netization. The shape of the loop in the tilted Γ_{24} phase can be explained assuming that for some reason domains are formed in this phase. Such assumption is supported by the fact that much lower domain wall energies were found in nonsymmetric phases.[33] Then the triangle and S-shaped $M(H)$ dependences reflect the evolution of the domain structure of the sample, and therefore the $\mathbf{M}^{\text{remnant}}$ measurement does not give information about the saturation magnetization. The value of the saturation magnetization, however, can be obtained by extrapolating the high-field linear $M(H)$ dependence down to zero field. The intersection of the line with the vertical axis gives the value of M for the saturation magnetization. The $M_a(T)$ and $M_c(T)$ dependencies calculated this way are plotted in Fig. 5. Now the gradual change in the magnetic moment projections is observed. The absolute value of **M** can be calculated (see inset in Fig. 7). Though not constant, $|\mathbf{M}|$ changes continuously and does not have jumps, as Fig. 3 might suggest. Thus the apparent contradiction is resolved. As mentioned, a change in the absolute value of **M** is due to the temperature-dependent magnetization of the Er ions in the molecular field of the iron subsystem.

Hysteresis loops for a magnetic field tilted in the (**a**,**c**) plane are shown in Fig. 6. Using the data for tilted field it was checked that the tilted projections of **M** are consistent with M_a and M_c measured at the same temperatures in experiments presented in Fig. 5.

Knowing the shape of the loops, a simpler and faster procedure to measure M_a and M_c can be implemented. From Fig. 4 it is observed that in a weak field, $H=50$ Oe, the magnetization value is approximately equal to saturation $M_{a,c}$ for all temperatures. Thus simple temperature sweeps at

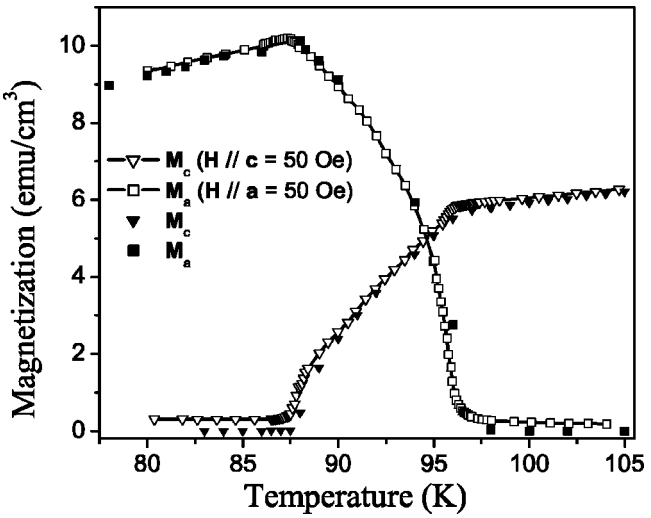

FIG. 5. $M_{a,c}(T)$ calculated from the magnetization loops as explained in the text (filled symbols); $M_{a,c}(T)$ measured in a temperature sweep at $H=50$ Oe as explained in the text (empty symbols).

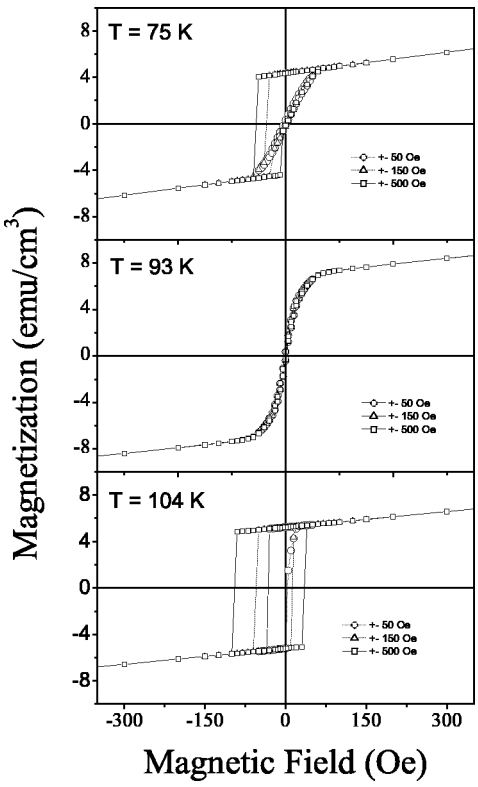

FIG. 6. Magnetization loops $M(H)$ for tilted direction of the external field.

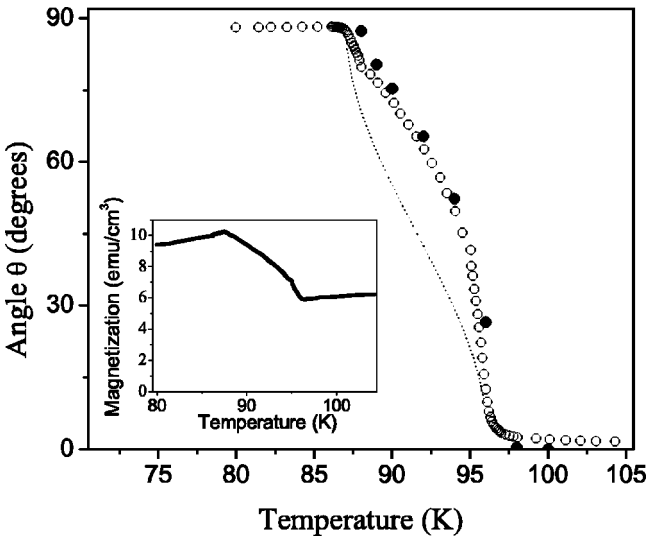

FIG. 7. Rotation angle $\theta(T)$ of the magnetization in the reorientation region $T\in[T_1,T_2]$ at zero external field. The angle is calculated from the **M** components measured at 50 Oe, as explained in the text (empty symbols), and from the components calculated from the magnetization loops (filled symbols). The dotted line represents a conventional mean-field theory result, given by Eq. (2). Inset, absolute value of magnetization $|\mathbf{M}|(T)$.

fixed field $H=50$ Oe directed along **a** or **c** axis give the corresponding components of **M**. Figure 5 shows $M_{a,c}$ measured in this manner. The difference between this measurement and the values obtained on the basis of loop analysis is insignificant. The main deficiency of the fast procedure is the parasitic nonzero magnetic moment measured in symmetric phases.

The hysteresis loops observed in our study allow for a precise direct measurement of the vector **M** components along **a** and **c** axis. Knowing M_a and M_c one can reconstruct the temperature dependence of $|\mathbf{M}|$ and the rotation angle θ:

$$|\mathbf{M}|=\sqrt{M_a^2+M_c^2},$$

$$\theta=\arctan\left(\frac{M_a}{M_c}\right).$$

The results are shown in Fig. 7.

IV. DISCUSSION

A. Phase diagram

The measurements of the saturation magnetization $M(T)$ required a study of the magnetization loops $M(H)$ at constant temperature. These hysteretic loops are a manifestation of the first-order OPT that the system undergoes in a magnetic field sweep through $H=0$. A first-order OPT of this kind is characteristic for any ferromagnet and simply means that its magnetic moment flips from ''up'' to ''down.'' To better understand the peculiarities of this transition in $ErFeO_3$, let us recall the form of the energy functional of an orthoferrite. It was explained in the Introduction that at zero external field the magnetization stays in the (**a**,**c**) plane for the investigated temperature range. If a magnetic field is applied in the same plane, this remains true for finite fields as well. Therefore, one angle θ (between **M** and **c** axis) determines the magnetization direction, and the free energy can be written as

$$\mathcal{F}(\mathbf{M},\mathbf{H})=\mathcal{F}_0(\theta)-\mathbf{M}\cdot\mathbf{H}.$$

Consider first the spontaneous magnetization **M** or its angle θ. As shown in Fig. 8, for $T>T_1$ the free energy $\mathcal{F}_0(\theta)$ has two equivalent minima at $\theta=0,\pi$. For $T<T_2$ equivalent minima are located at $\theta=\pm\pi/2$. Finally, for $T\in[T_2,T_1]$ the energy has four equivalent minima at $\pm\theta(T),\pi\pm\theta(T)$. At T_1 and T_2 the angle $\theta(T)$ reaches 0 and $\pi/2$, respectively, and equilibrium points merge pairwise. The positions of equilibria in the (M_a,M_c) plane are symmetric with respect to **a** and **c** axes, which follows from the symmetry of the orthoferrite.

An application of the external magnetic field generally lifts the degeneracy of the equilibria. The lowest-energy state is related to the equilibrium, with the vector **M** being closest to **H**. If **H** changes sign, the state with the $-\mathbf{M}$ moment becomes the lowest-energy state. In a thermodynamic sense the jump from **M** to $-\mathbf{M}$ (first-order transition) happens exactly at $H=0$ since the energies of **M** and $-\mathbf{M}$ states are equal by symmetry at this point. Of course, the **M** state remains metastable, and therefore, as in any first-order transition, a hysteresis is possible. There is, however, a special direction of the magnetic field, in which no transition happens at $H=0$. This is a direction for which the degeneracy

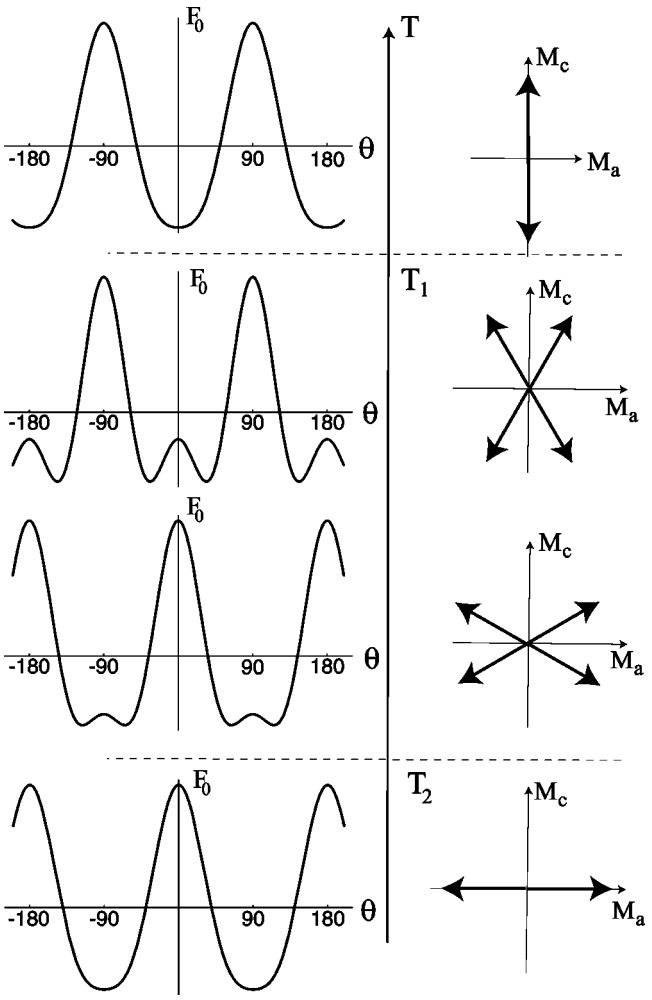

FIG. 8. Magnetic energy and equilibrium direction of magnetization in $ErFeO_3$ in different phases.

between the states is not lifted. Such situation is only possible when two conditions are fulfilled. First, the spontaneous magnetization has to have two (as opposed to four) equilibrium directions, i.e., for $T<T_2$ or $T>T_1$. This is necessary because when four equilibria are present, any direction of **H** will lift the fourfold degeneracy to either a nondegenerate situation or two doubly degenerate equilibria, and thus make possible a transition at $H=0$. Second, the field has to be directed perpendicular to the magnetization, $\mathbf{H}\perp\mathbf{M}$ to make the energy of two equilibria equal for any magnitude of the field.

What do these arguments mean for a three-dimensional (H_a,H_c,T) phase diagram of the orthoferrite? The two-dimensional cross sections (H_a,T) and (H_c,T) are well known and shown in Figs. 9(a,b).[3,13,14,21] For $\mathbf{H}\|c$, the special situation discussed in the preceding paragraph arises when $\mathbf{M}\|\mathbf{a}$, i.e., for $T<T_2$ (observe the absence of the thick first-order $H=0$ line there). For $\mathbf{H}\|a$, the special situation happens when $\mathbf{M}\|\mathbf{c}$, i.e., for $T>T_1$. This is well illustrated by our measurements on Fig. 4. For example, as shown in Sec. III for the $\mathbf{H}||a$ case [Fig. 4(a)], a nonzero saturation moment below T_1 is observed. Above T_1 the $M(H)$ dependence is linear which gives $M_c=0$ at $H=0$ and thus there is no jump and no phase transition.

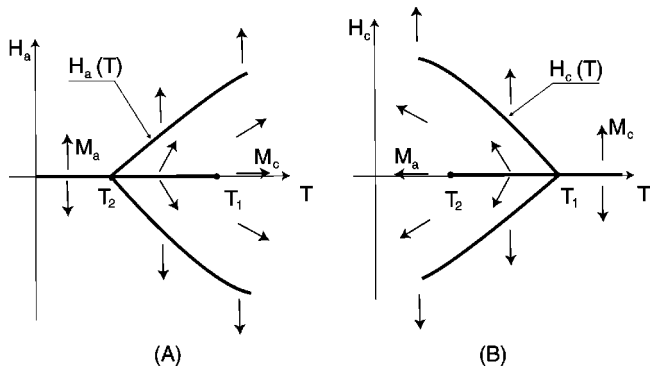

FIG. 9. Two-dimensional phase diagrams (a) in the (H_a,T) and (b) in the (H_c,T) planes.

Before going to the 3D diagram, consider the field-induced transition at $H=H_{a,c}(T)$ also shown in Figs. 9(a,b).[3,13,14,21,28] This well-known second-order transition is characterized by the field-induced merger of two equivalent equilibria. But such equivalent equilibria exist only for $\mathbf{H}\|a$ or $\mathbf{H}\|\mathbf{c}$. For a generic direction of **H** one equilibrium is always an absolute minimum and the rest are metastable states which play no role in the thermodynamic sense.[29] This is why in the 3D diagram the field-induced transition will happen not on two-dimensional surfaces, but only on one-dimensional curves lying in the (H_a,T) and (H_c,T) planes.

With all of the above said, the 3D phase diagram is presented in Fig. 10. The shaded planar regions (wedges) represent planes of first-order transitions. Upon passing through one of these wedges, a component of **M** jumps; more precisely the M_c component jumps when the horizontal wedge is crossed and the M_a component jumps when the vertical wedge is crossed. The boundaries of the wedges are the second-order transition lines. As the system passes through a

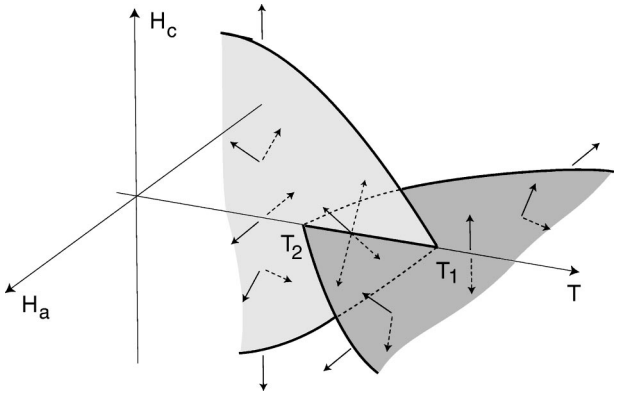

FIG. 10. Phase diagram of $ErFeO_3$ in the (H_a,H_c,T) space. Two wedges, lightly hatched vertical and gray horizontal, are the surfaces of a first-order transition. Component M_c jumps upon crossing the horizontal wedge and component M_a jumps upon crossing the vertical wedge. Between T_1 and T_2 crossing the $H=0$ line always leads to a first-order transition. Above T_1 and below T_2, transition upon crossing $H=0$ can be avoided if one moves exactly in the plane of the corresponding wedge.

wedge close to the wedge boundary, the jump of **M** decreases and disappears at the boundary.

The magnetization loops measured for **H** tilted in the (**a**,**c**) plane (Fig. 6) supports the proposed 3D phase diagram. They show that for a generic direction of **H** there is always a first-order transition upon sweeping through $H=0$. Unlike Fig. 4, no region with a linear $M(H)$ dependence is observed here. This result is in complete accord with the physical picture that leads to Fig. 10. Indeed, between T_1 and T_2, four equilibria are present so there are no ''special directions'' of magnetic field that can destroy the first-order transition at $H=0$. Outside of the $[T_2,T_1]$ interval $\mathbf{H}\perp\mathbf{M}$ cannot be achieved for the tilted field. As a result, for a generic direction of **H** in the (**a**,**c**) plane the special conditions are never fulfilled and the first-order transition is always present. In the 3D diagram this statement corresponds to the fact that going along a tilted line through $H=0$ one always crosses at least one of the wedges (sometimes both), thus going through a first-order transition.

B. Domain structure

As any magnetic first-order transition, the OPT at $H=0$ may be masked by the presence of domains. If domains are formed, the transition can proceed without hysteresis. This is actually the situation that is seen in our experiment for $T\in[T_2,T_1]$. The S-shaped nonhysteretic or triangle curves observed roughly between ± 50 Oe are most probably a consequence of the multidomain state of the sample. Indeed, as observed in previous investigations,[30] these curves cannot be explained by the magnetization rotation in a single-domain state since, for anisotropy constants of $ErFeO_3$,[31] the characteristic width of the loop, determined by Slonczewski's astroid curve,[32] would be of the order $K/M\approx 1$ kOe. Note that even though K_u goes through zero, the presence of constant K_b ensures the large characteristic scale. Thus monodomain rotation of **M** is incompatible with 50 Oe switching scale observed in our experiment. The shape of the loops therefore depends on the domain structure, energy of domain wall formation, and the shape of the sample. Another signature of the presence of a domain structure is the dependence of the loop shape on the amplitude of magnetic field sweep. This effect is seen in Fig. 6.

By extrapolating the high-field linear dependence $M(H)$ to $H=0$ and obtaining a nonzero value of M, the presence of the underlying first-order transition is revealed.

In the $T>T_1$ and $T<T_2$ intervals rectangular loops are observed. This means that no stable domain structure is formed, and switching happens between two monodomain configurations (though the mechanism of switching may include dynamic domain wall motion).

The signature of domain formation inside the $[T_2,T_1]$ interval and the absence of such outside it was observed in our experiments for all orientations of the magnetic field, including the field tilted in the (**a**,**c**) plane (see Figs. 4 and 6). This result probably reflects some intrinsic difference between the domain walls in the tilted Γ_{24} phase on one hand and the symmetric Γ_4 and Γ_2 phases on the other. Such difference is likely to be a consequence of the symmetry difference between the phases and requires a closer investigation. A similar difference in the domain wall energy between the symmetric and nonsymmetric phases has been reported.[33,34]

C. Temperature dependence of the rotation angle

To date these measurements are the most accurate and direct experimental approach known to the authors to give the spin rotation angle $\theta(T)$ for erbium orthoferrite (see Fig. 7). The results confirm the continuous rotation of **M** in the reorientation region. The $\theta(T)$ dependence in orthoferrites is often described by a mean field Landau theory. In the usual approach[3,13–19] the magnetization is assumed to have constant magnitude $|M|$ and the free energy is a function of the rotation angle only:

$$\mathcal{F}=\mathcal{F}_0+\frac{1}{2}K_u(T)\cos(2\theta)+K_b\cos(4\theta). \tag{1}$$

For $K_b>0$ the reorientation region is defined by inequalities

$$-8K_b<K_u(T)<8K_b,$$

and within it the rotation angle is given by

$$\tan^2\theta(T)=\frac{8K_b+K_u(T)}{8K_b-K_u(T)}.$$

It is also assumed, and can be verified in many orthoferrites,[13,17,19,21,24] that within this interval $K_u(T)$ has an approximately linear dependence on T,

$$K_u(T)=8K_b\xi(T),$$

$$\xi(T)=\frac{(T_1+T_2)/2-T}{(T_1-T_2)/2}$$

and K_b is approximately temperature independent. Then the angle is given by

$$\tan\theta=\sqrt{\frac{1+\xi}{1-\xi}}. \tag{2}$$

When OPT temperatures are known (for $ErFeO_3$ $T_1=97$ K, $T_2=88$ K), this formula has no fitting parameters. The resulting $\theta(T)$ is shown on Fig. 7 as a dotted line. It is seen that Eq. (2) does not describe the experimental findings. This is not very surprising, since our measurement shows that magnetic moment is not the same in the two phases, but rather changes during the reorientation process. From T_1 to T_2 it changes by a factor $F_a(T_2)/F_c(T_1)\approx 1.72$. Thus at least some assumptions that lead to Eq. (2) are violated in the material.

How can the magnetization of erbium orthoferrite change by about 70% in the 10 K temperature interval if the reorientation happens so far below the Neel temperature of the material? This change in the magnitude of $|\mathbf{M}|$ is assumed to be due to the change of the Er magnetization **m**, while the iron magnetization **F** indeed does not change.[1,4,6,8] In the reorientation interval erbium ions are paramagnetic and only partially magnetized by the molecular field of the iron sub-

system. Phenomenologically, the angle dependence of $|\mathbf{M}|$ can be reproduced by assuming that the susceptibilities of the Er ions to the molecular field in **a** and **c** directions are different:

$$m_a = \chi_a^{\mathrm{Er}} F_a ,$$

$$m_c = \chi_c^{\mathrm{Er}} F_c . \tag{3}$$

For $\chi_c^{\mathrm{Er}} \neq \chi_a^{\mathrm{Er}}$, $|\mathbf{m}|$ (and accordingly $|\mathbf{M}|$) will change as **F** rotates. It should be underscored that in this approach $|\mathbf{m}|$ changes not due to a strong temperature dependence of χ's, but because different components of the susceptibility tensor are relevant for the high and low ends of the reorientation interval.

To describe this mechanism in mean-field theory framework we consider the free-energy functional

$$\tilde{\mathcal{F}} = \tilde{\mathcal{F}}_0 + \frac{1}{2} K_u(T) \cos(2\theta_F) + K_b \cos(4\theta_F)$$

$$- \beta (F_a \chi_a^{\mathrm{Er}} m_a + F_c \chi_c^{\mathrm{Er}} m_c) + \frac{\beta}{2} \mathbf{m}^2 \tag{4}$$

where θ_F is the rotation angle of **F**, $F_a = F \sin\theta_F$, $F_c = F \cos\theta_F$. The third term in Eq. (4) describes the influence of iron molecular field on erbium magnetization, and the fourth term with $\beta > 0$ ensures that erbium subsystem is paramagnetic.

Energy functionals with explicit Er-Fe interaction terms were introduced following the idea[1] that it is this interaction that drives the spin-reorientation transitions. Mean-field theories accounting for the interaction of all eight (four iron and four erbium) sublattices in the magnetic structure of the orthoferrites[8] and theories adopting the ferromagnetic moment approximation[6,4] were put forward. However, in previous research the main goal was to explain the existence of the two second-order transitions, and the temperature dependence of the rotation angle, which is of primary interest for us, was not considered.

Minimization of $\tilde{\mathcal{F}}$ with respect to m_a and m_c indeed gives Eqs. (3). When evaluated at the equilibrium values of **m**, Eq. (4) gives

$$\tilde{\mathcal{F}} = \tilde{\mathcal{F}}_0 + \frac{1}{2} K_u \cos(2\theta_F) + K_b \cos(4\theta_F)$$

$$- \frac{\beta}{2} [(\chi_a^{\mathrm{Er}})^2 F_a^2 + (\chi_c^{\mathrm{Er}})^2 F_c^2]$$

$$= \tilde{\mathcal{F}}_0' + \frac{1}{2} K_u' \cos(2\theta_F) + K_b \cos(4\theta_F) \tag{5}$$

with new coefficients defined as

$$\tilde{\mathcal{F}}_0' = \tilde{\mathcal{F}}_0 - \frac{\beta F^2}{4} [(\chi_a^{\mathrm{Er}})^2 + (\chi_c^{\mathrm{Er}})^2]$$

$$K_u' = K_u - \frac{\beta F^2}{2} [(\chi_c^{\mathrm{Er}})^2 - (\chi_a^{\mathrm{Er}})^2]. \tag{6}$$

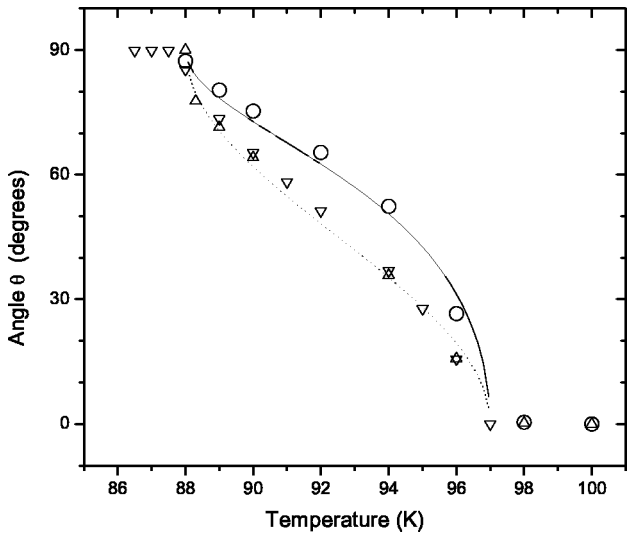

FIG. 11. Theoretical fits of the temperature dependence of the θ and θ_F. Experimental values of θ are shown by circles, a fit with formula (7) is given by a full line. Upward pointing triangles are experimental values of θ_F calculated as $\arcsin[M_a/M_a(T_2)]$ and downward pointing triangles as $\arccos[M_c/M_c(T_1)]$. We see that both methods indeed give the same θ_F. The dotted line is given by formula (2).

Equation (5) has the same form as Eq. (1) and thus leads to the same picture of two phase transitions, whether the effective constant K_u' depends on temperature due to the temperature dependence of iron subsystem anisotropy constant K_u (Refs. 3,13–18 and 19) or due to the temperature dependence of χ^{Er}.[6,4] Due to the renormalization of K_u given by Eq. (6), the OPT temperatures are now different, but in terms of the actual T_1, T_2 known from experiment, the angle θ_F is given by the same Eq. (2) as before. The angle of rotation of the total magnetization **M** is obtained from

$$\tan\theta = \frac{M_a}{M_c} = \left(\frac{1+\chi_a^{\mathrm{Er}}}{1+\chi_c^{\mathrm{Er}}} \right) \frac{F_a}{F_c} = \left(\frac{1+\chi_a^{\mathrm{Er}}}{1+\chi_c^{\mathrm{Er}}} \right) \tan\theta_F .$$

Taking into account that $M(T_1) = M_c(T_1) = (1+\chi_c^{\mathrm{Er}})F$ and $M(T_2) = M_a(T_2) = (1+\chi_a^{\mathrm{Er}})F$, this formula can be rewritten as

$$\tan\theta = \frac{M_a(T_2)}{M_c(T_1)} \tan\theta_F .$$

As a result, the modified mean-field theory predicts

$$\tan\theta = \frac{M_a(T_2)}{M_c(T_1)} \sqrt{\frac{1+\xi}{1-\xi}}. \tag{7}$$

Again for this formula there are no adjustable parameters that are not determined from the experiment. Using the relation $M_a(T_2)/M_c(T_1) \approx 1.72$ the theoretical curve (full line in Fig. 11) and the observed data are in very good agreement. Slight deviation may be ascribed to small changes of $\chi_{a,c}^{\mathrm{Er}}$ with the temperature. As seen from Fig. 5 the magnetization does change with temperature even in the symmetric phases. This change, however, is less than 5–10% and in the first

approximation could be neglected in comparison with the reorientation-induced change of $|\mathbf{M}|$. Small temperature dependence of K_b may also play a role. The present accuracy of experiment is insufficient to determine the source of small differences between the data and expression (7). It is worth mentioning that the ratio of the slopes of $M_a(T)$ dependence in the Γ_2 phase and $M_c(T)$ dependence in the Γ_4 phase,

$$\frac{(dM_a/dT)_{\Gamma_2}}{(dM_c/dT)_{\Gamma_4}} = \frac{(d\chi_a^{\mathrm{Er}}/dT)_{\Gamma_2}}{(d\chi_c^{\mathrm{Er}}/dT)_{\Gamma_4}} \approx 1.76,$$

within experimental error happens to be the same as the $M_a(T_2)/M_c(T_1)$ ratio. This fact may have implications for the future theory of Er magnetism.

The fit of formula (7) with no adjustable parameters is a very strong support for this model. At the same time it means that any additional information about χ_a^{Er} and χ_b^{Er} cannot be extracted from the fitting procedure. In particular, according to Ref. 1 erbium ions are magnetized opposite to the iron ions for all temperatures. In accord with this statement, $|\mathbf{M}|$ decreases with decreasing temperature in both symmetric phases (see Fig. 5), and for sufficiently low temperatures (not studied in this work) $ErFeO_3$ is known to have a compensation point with $\mathbf{M}=\mathbf{F}+\mathbf{m}=0$. The presence of the compensation point would be impossible if **F** and **m** pointed in the same direction. Thus, both χ's are in fact negative, and their absolute values satisfy $|\chi_a^{\mathrm{Er}}|<|\chi_c^{\mathrm{Er}}|$ to produce the increase of $|F|$. But the fit would work equally well if χ's were positive with $|\chi_a^{\mathrm{Er}}|>|\chi_c^{\mathrm{Er}}|$. The only thing that matters is the ratio $(1+\chi_a^{\mathrm{Er}})/(1+\chi_c^{\mathrm{Er}})=M_a(T_2)/M_c(T_1)$.

However the dependence of $\theta_F(T)$ can also be extracted from the data. From the definition of this angle

$$\sin\theta_F = \frac{F_a}{F} = \frac{M_a}{(1+\chi_a^{\mathrm{Er}})F} = \frac{M_a}{M_a(T_2)}$$

$$\cos\theta_F = \frac{F_c}{F} = \frac{M_c}{(1+\chi_c^{\mathrm{Er}})F} = \frac{M_c}{M_c(T_1)}.$$

Plotting $\arcsin[M_a/M_a(T_2)]$ and $\arccos[M_c/M_c(T_1)]$ (Fig. 11) it can be demonstrated that both procedures give the same angle and that it can be fitted by Eq. (2), as expected from the modified mean-field theory.

V. CONCLUSIONS

The magnetization of $ErFeO_3$ was measured by a SQUID magnetometer. The precision of the experiment allowed the measurement of the temperature dependence of the magnetic moment rotation angle and absolute value, and uncovered a significant change of Er magnetization in the reorientation region. By taking the angle dependence of the erbium magnetism into account in the mean-field theory framework, an excellent agreement with experiment was achieved.

The first-order phase transition at $H=0$ was analyzed on the basis of a 3D phase diagram. The difference between symmetric and nonsymmetric directions of magnetic field was explained. A drastic difference in the shape of the hysteresis loops in the reorientation region and outside of this region was observed and discussed from the point of view of domain structure formation in the phases of different symmetry.

ACKNOWLEDGMENTS

This work was supported by the Science and Technology Center of Ukraine. The work of Y.B. at Argonne National Laboratory was supported by the U.S. Department of Energy, Office of Science, under Contract No. W-31-109-ENG-38.

*Electronic address: tsymbal@sova.fti.ac.donetsk.ua

[1] R. White, J. Appl. Phys. **40**, 1061 (1969).
[2] K.P. Belov, A.K. Zvezdin, A.M. Kadomtseva, and R.Z. Levitin, Usp. Fiz. Nauk **119**, 447 (1976) [Sov. Phys. Usp. **19**, 574 (1976)].
[3] K.P. Belov, A.K. Zvezdin, A.M. Kadomtseva, and R.Z. Levitin, *Orientation Phase Transitions in Rare Earth Magnetic Materials* (Nauka, Moscow, 1979) (in Russian).
[4] D. Treves, J. Appl. Phys. **36**, 1033 (1965).
[5] E.M. Gyorgy, J.P. Remeika, and F.B. Hagedorn, J. Appl. Phys. **39**, 1369 (1968).
[6] J. Sirvardiere, Solid State Commun. **7**, 1555 (1969).
[7] R.M. Hornreich and I. Yaeger, Int. J. Magn. **4**, 71 (1973).
[8] T. Yamaguchi, J. Phys. Chem. Solids **35**, 479 (1974).
[9] R.E. Bornfreund, D.C. Khan, P.E. Wigen, M. Parvadi-Horvath, J.B. Ings, and R.F Belt, J. Magn. Magn. Mater. **151**, 181 (1995).
[10] A. Bombik and A.W. Pacyna, J. Magn. Magn. Mater. **220**, 18 (2000).
[11] V.D. Buchel'nikov, N.K. Danshin, A.I. Linnik, L.T. Tsymbal, V.G. Shavrov, JETP **122**, 122 (2002).
[12] Ya.B. Bazaliy, L.T. Tsymbal, A.I. Linnik, N.K. Dan'shin, A.I. Izotov, and P.E. Wigen, Physica B **329-333**, 1257 (2003).
[13] H. Horner and C.M. Varma, Phys. Rev. Lett. **20**, 845 (1968).
[14] J.R. Shane, Phys. Rev. Lett. **20**, 728 (1968).
[15] F.B. Hagedorn, E.M. Gyorgy, R.C. LeCrow, J.C. Hensel, and J.P. Remeika, Phys. Rev. Lett. **21**, 364 (1968).
[16] R.D. Pierce, R. Wolfe, and L.G. Van Uitert, J. Appl. Phys. **40**, 1241 (1969).
[17] K.P. Belov, R.A. Volkov, B.P. Goranskii, A.M. Kadomtseva, and V.V. Uskov, Fiz. Tverd. Tela (Leningrad) **11**, 1148 (1969) [Sov. Phys. Solid State **11**, 935 (1969)].
[18] L.M. Levinson, M. Luban, and S. Shtrikman, Phys. Rev. **187**, 715 (1969).
[19] M. Abe, M. Gomi, K. Shono, Y. Mori, and S. Nomura, Jpn. J. Appl. Phys. **16**, 279 (1977).
[20] F.B. Hagedorn and E.M. Gyorgy, Phys. Rev. **174**, 540 (1968).
[21] W.J. Schaffer, R.W. Bene, and R.M. Walser, Phys. Rev. B **10**, 255 (1974).
[22] N.M. Kovtun, A.S. Karnachev, E.E. Solov'ev, A.Ya. Chervonenkis, and A.A. Shemyakov, Fiz. Tverd. Tela (Leningrad) **14**, 2150 (1973) [Sov. Phys. Solid State **14**, 1856 (1973)].
[23] R.W. Grant and S. Geller, Solid State Commun. **7**, 1291 (1969).

[24] S. Kagoshima and S. Takayama, J. Phys. Soc. Jpn. **29**, 793 (1970).
[25] L.T. Tsymbal and A.I. Izotov, Zh. Éksp. Teor. Fiz. **102**, 963 (1992) [Sov. Phys. JETP **75**, 525 (1992)].
[26] V.D. Buchel'nikov, N.K. Dan'shin, L.T. Tsymbal, and V.G. Shavrov, Usp. Fiz. Nauk **166**, 585 (1996) [Phys. Usp. **39**, 547 (1996)].
[27] I.E. Dikshtein, V.V. Tarasenko, and V.G. Shavrov, Fiz. Tverd. Tela (Leningrad) **19**, 1107 (1997) [Sov. Phys. Solid State **19**, 644 (1977)].
[28] K.P. Belov *et al.*, Phys. Status Solidi A **36**, 415 (1976).
[29] Here we do not discuss the breakdown of the metastable states. In the regimes with two spontaneous equilibria the boundary of the metastable state existence is given by the famous astroid curve (Ref. 32). For the four equilibrium state the situation is more complicated.
[30] S. Reich, S. Shtrikman, and D. Treves, J. Appl. Phys. **36**, 140 (1965).
[31] The anisotropy constants of orthoferrites [see Eq. (1) for definitions] far from the spin-reorientation transition are of the order $K_u \sim 10^5$ erg/cm^3, $K_b \sim (10\text{–}30\%)K_u$ (Ref. 1,6 and 17).
[32] J.C. Slonczewski, IBM Research Memorandum No. 003.111.224 (1956); Also see L.D. Landau and E.M. Lifshitz, *Electrodynamics of Continuous Media* (Pergamon, New York, 1960), Sec. 37, pp. 150–151.
[33] F.C. Rossol, J. Appl. Phys. **39**, 5263 (1968).
[34] F.C. Rossol, J. Appl. Phys. **40**, 1082 (1969).